



Behavior of iron in (Mg,Fe)SiO₃ post-perovskite assemblages at Mbar pressures

Jennifer M. Jackson,¹ Wolfgang Sturhahn,^{1,2} Oliver Tschauner,^{1,3} Michael Lerche,⁴ and Yingwei Fei⁵

Received 18 February 2009; accepted 30 March 2009; published 19 May 2009.

[1] The electronic environment of the iron sites in post-perovskite (PPv) structured (⁵⁷Fe,Mg)SiO₃ has been measured in-situ at 1.12 and 1.19 Mbar at room temperature using ⁵⁷Fe synchrotron Mössbauer spectroscopy. Evaluation of the time spectra reveals two distinct iron sites, which are well distinguished by their hyperfine fields. The dominant site is consistent with an Fe³⁺-like site in a high spin state. The second site is characterized by a small negative isomer shift with respect to α -iron and no quadrupole splitting, consistent with a metallic iron phase. Combined with SEM/EDS analyses of the quenched assemblage, our results are consistent with the presence of a metallic iron phase co-existing with a ferric-rich PPv. Such a reaction pathway may aid in our understanding of the chemical evolution of Earth's core-mantle-boundary region. **Citation:** Jackson, J. M., W. Sturhahn, O. Tschauner, M. Lerche, and Y. Fei (2009), Behavior of iron in (Mg,Fe)SiO₃ post-perovskite assemblages at Mbar pressures, *Geophys. Res. Lett.*, 36, L10301, doi:10.1029/2009GL037815.

1. Introduction

[2] Ferromagnesium silicate post-perovskite (PPv) is suggested to co-exist with CaSiO₃ perovskite and (Mg,Fe)O in Earth's D'' layer [Mao et al., 2004; Murakami et al., 2004; Oganov and Ono, 2004; Shim et al., 2004]. The implications of such a phase transition has been treated in seismological interpretations [Sidorin et al., 1999; Hernlund et al., 2005; van der Hilst et al., 2007] and dynamical simulations [Nakagawa and Tackley, 2004; Lassak et al., 2007]. The electronic charge and spin state of iron in mantle phases may influence its hosts' physical and chemical properties, such as in the case of (Mg,Fe)O ferropericlasite [Shannon and Prewitt, 1969; Gaffney and Anderson, 1973; Lin et al., 2005, 2006b; McCammon, 2006; Crowhurst et al., 2008]. However, the electronic charge and spin state of iron in magnesium silicate perovskite (Pv) and PPv is not very well understood. Based on analysis of quenched samples, the electronic charge states of iron (e.g., Fe²⁺

and Fe³⁺) in Pv may affect the presence of metallic iron [Frost et al., 2004; Kobayashi et al., 2005; Auzende et al., 2008], thereby potentially affecting siderophile element partitioning in the lower mantle.

[3] Most studies to determine the behavior of iron in PPv have been limited to analysis of quenched amorphized phases from high pressure-temperature (PT) diamond-anvil-cell runs [Kobayashi et al., 2005; Murakami et al., 2005; Sinmyo et al., 2006; Auzende et al., 2008; Sinmyo et al., 2008a, 2008b]. However, there is no a priori reason why the behavior of iron in a quenched amorphous compound reflects the behavior of its high-PT crystalline form. In-situ determination of the charge and spin states of iron in deep Earth phases [Badro et al., 2003, 2004; Jackson et al., 2005; Li et al., 2006; Lin et al., 2006a, 2008; McCammon et al., 2008] is a necessary step in order to formulate accurate physical and chemical scenarios for these regions.

2. Sample Synthesis

[4] A sintered platelet of polycrystalline orthoenstatite-structured (⁵⁷Fe_{0.13}Mg_{0.87})SiO₃, characterized by >95% high-spin divalent iron [Jackson et al. 2009], with lateral dimensions of $\sim 30 \times 30 \mu\text{m}^2$ and a thickness of $< 10 \mu\text{m}$ was loaded into the sample chamber of a pre-indented rhenium gasket in a sandwich configuration with dehydrated NaCl as a pressure medium and marker. Gold was placed ~ 20 microns from the sample for use as an additional pressure marker. Two diamond anvil cells equipped with beveled anvils were prepared in this manner, then pressurized to over one megabar. The high temperature synthesis of PPv was performed with the CO₂-laser heating system at the University of Nevada, Las Vegas. Angle-dispersive powder x-ray diffraction ($\lambda = 0.34531 \text{ \AA}$) at the High-Pressure Collaborative Access Team was used to confirm the synthesis of a post-perovskite structure consistent with CaIrO₃-type (Cmcm) and 2×1 (P2₁/m) PPv symmetries (see Figure S1 of the auxiliary material) [Oganov et al., 2005; Tschauner et al., 2008].¹ The lattice parameters of NaCl-B2 and gold were determined from these measured spectra to determine the pressures in the two different DACs, namely $P = 1.19 \pm 0.04$ Mbar and $P = 1.12 \pm 0.04$ Mbar, respectively [Dewaele et al., 2004; Fei et al., 2007]. Including the effects of thermal pressure, the samples likely experienced an additional ~ 10 GPa of pressure while heated. More details on sample preparation, synthesis,

¹Seismological Laboratory, Division of Geological and Planetary Sciences, California Institute of Technology, Pasadena, California, USA.

²Advanced Photon Source, Argonne National Laboratory, Argonne, Illinois, USA.

³High Pressure Science and Engineering Center, Department of Physics, University of Nevada, Las Vegas, Nevada, USA.

⁴HPSynC, Argonne National Laboratory, Argonne, Illinois, USA.

⁵Geophysical Laboratory, Carnegie Institution of Washington, Washington, D. C., USA.

¹Auxiliary materials are available in the HTML. doi:10.1029/2009GL037815.

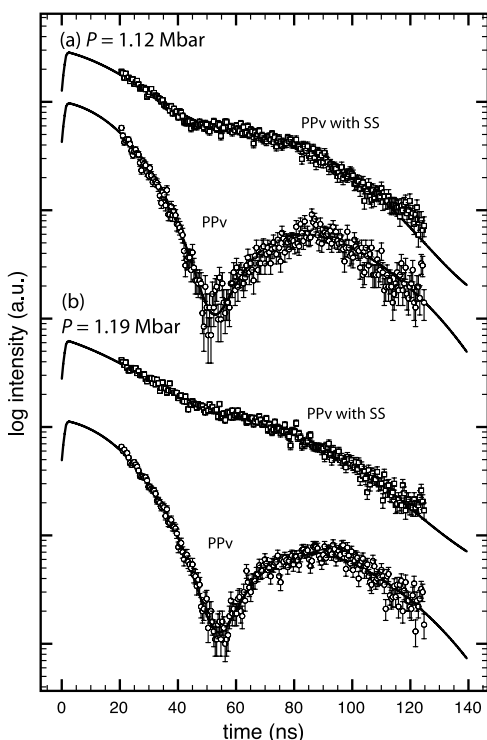


Figure 1. Synchrotron Mössbauer spectra of ($^{57}\text{Fe,Mg}$)- SiO_3 -PPv with and without stainless steel (SS) prepared in two different diamond-anvil-cells, at (a) $P = 1.12$ Mbar (synthesized at 1200 ± 200 K) and (b) $P = 1.19$ Mbar (synthesized at 1350 ± 200 K). The lines through the data represent the best-fit hyperfine parameters (Table 1). The normalized χ^2 values for the fits are all around 1.3.

and pressure determination can be found in the auxiliary material.

3. Synchrotron Mössbauer Spectroscopy (SMS) Experiments and Data Evaluation

[5] SMS experiments were performed at beamline 3-ID-B of the Advanced Photon Source. The hyperfine parameters of iron are directly determined by analysis of the SMS time spectra. Additional constraints on the isomer shift (IS) and the quadrupole splitting (QS) of the sample and its thickness were provided by placing a natural stainless steel (SS) foil with a physical thickness of $3 \mu\text{m}$ in the x-ray beam path [Alp *et al.*, 1995]. Therefore, spectra were collected with and without SS foil with collection times of ~ 2 hours/spectrum (Figures 1a and 1b). Spectra without SS foil were evaluated first, to constrain the quadrupole splittings and weights of the sites. With this information, the isomer shifts

of all sites were determined using the spectra containing the SS foil reference. The effective thickness, η , of the samples were determined to be ~ 0.03 , thus having negligible effects on the time spectra. All IS values are relative to α -iron; the IS of stainless steel relative to α -iron is -0.09 mm/s [Hawthorne, 1988]. Details of experimental set-up and data analysis using CONUSS as given by Jackson *et al.* [2009] and Sturhahn [2000], respectively.

[6] Two sites that are well distinguished by their hyperfine fields dominate the spectra. One site, representing 71% of the total iron (site #1), is characterized by a low QS around 0.74 mm/s and an IS of 0.45 mm/s (Figures 1a and 1b and Table 1). These QS and IS values are consistent with previous reports on the behavior of high-spin Fe^{3+} in similar coordination environments [McCammon, 1997; Jackson *et al.*, 2005; Li *et al.*, 2006] (see Table S1). The remaining 29% of the iron (site #2) is characterized by an IS of about -0.16 mm/s with no field gradient. We identify this site as a metallic iron phase [Pipkorn *et al.*, 1964]. To our knowledge, no oxide or silicate exhibits such a small negative IS [Dyar *et al.*, 2006]. Transmission spectra were calculated from CONUSS using these best-fit hyperfine parameters (Figure S2).

[7] We note that the addition of a minority site contributing not more than 5% with a high QS of around 4 mm/s could be incorporated into our above model without changing our normalized χ^2 values. This minority site is suggestive of a Fe^{2+} -like site in a non-zero spin state in an 8–12 coordinated site, which has been observed in all existing Mössbauer measurements on Pv at megabar pressures [Jackson *et al.*, 2005; Li *et al.*, 2006; Lin *et al.*, 2008; McCammon *et al.*, 2008]. One can see that an addition of greater than 5% of a high QS component distinctive to Pv produces an observable mis-match to the SMS spectra (see Figure S3).

4. Iron-Rich Clusters in Post-perovskite Assemblages

[8] In most iron-bearing oxide and silicate phases, oxygen fugacity controls the valence state of iron in the host phase. For example, the formation of Fe_2O_3 , Fe_3O_4 , FeO , and Fe metal at ambient pressure are typically controlled by the available oxygen. In contrast to these phenomena, the amount of Fe^{3+} in silicate perovskite is suggested to be independent of oxygen fugacity and correlated with Al^{3+} content [Lauterbach *et al.*, 2000]. It has been suggested that the formation of Fe^{3+} in aluminous silicate perovskite is achieved by self-reduction of Fe^{2+} to form iron metal and Fe^{3+} via the following simplified reaction: $3\text{Fe}^{2+} \rightarrow 2\text{Fe}^{3+} + \text{Fe}^0_{\text{metal}}$ [Frost *et al.*, 2004]. Analytical transmission electron microscopy measurements performed on quenched

Table 1. Best Fit Hyperfine Parameters Obtained From Fits to the SMS Time Spectra^a

Pressure (Mbar)	Fe^{3+} -like (Site #1) PPv				Metallic Iron Phase (Site #2)		
	Wt (%)	QS (mm/s)	IS (mm/s)	FWHM (mm/s)	Wt (%)	IS (mm/s)	FWHM (mm/s)
1.12(4)	71	0.74(1)	0.45(3)	0.39(1)	29(2)	$-0.16(1)$	0.6
1.19(4)	71	0.73(1)	0.45(2)	0.38(1)	29(2)	$-0.14(2)$	0.6

^aWt, weight fraction of the site; QS, quadrupole splitting; IS, isomer shift (relative to α -iron); FWHM, full width at half maximum of the IS. Parameters with error values were varied in the fits. The weights are normalized to 100%. Uncertainties are given in parenthesis at the 90% confidence level for the last reported significant digit. The normalized χ^2 values for the fits are all around 1.3.

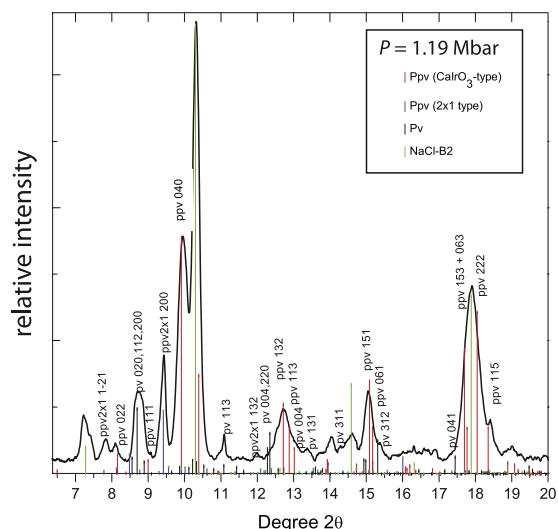
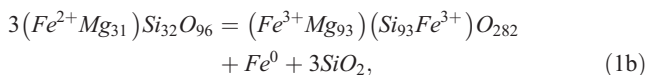
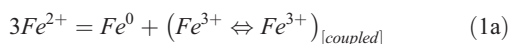


Figure 2. Integrated X-ray diffraction ($\lambda = 0.34531 \text{ \AA}$) 2θ spectrum of $(^{57}\text{Fe},\text{Mg})\text{SiO}_3\text{-PPv}$ at $P = 1.19 \text{ Mbar}$ at 300K (raw spectrum can be found in Figure S1). The calculated peak positions and proportions are as follows: $60 \pm 10\%$ PPv – CaIrO_3 structure ($Cmcm$), $30 \pm 10\%$ PPv 2×1 - kinked structure ($P2_1/m$), $10 \pm 10\%$ Pv – perovskite ($Pbnm$), and NaCl - CsCl-B2 structure ($Pm\bar{3}m$) (see auxiliary material for more details).

samples from multi-anvil [Lauterbach *et al.*, 2000; Frost *et al.*, 2004] and diamond-anvil-cell experiments [Kobayashi *et al.*, 2005; Auzende *et al.*, 2008] have shown that such a reaction is possible in Al-bearing and in Al-free silicate Pv. Recent theoretical investigations have also suggested that the formation of metallic iron could be energetically favorable [Zhang and Oganov, 2006]. In Al-free systems, the reaction would proceed as follows:



with an enthalpy, ΔH , equal to -2.266 eV for Pv and -2.575 eV for PPv [Zhang and Oganov, 2006]. However, there has been no strong experimental evidence for such a reaction involving PPv. According to Kobayashi *et al.* [2005], metallic iron was detected in an analytical transmission electron microscopy analysis of a quenched amorphous PPv-bearing assemblage from $P \sim 1.2 \text{ Mbar}$, but the grains were too small to be confidently associated with a particular phase. According to Auzende *et al.* [2008], metallic iron was detected in similar quenched phase assemblies from $P < 1 \text{ Mbar}$, but was not observed in their quenched assembly from $P \sim 1.2 \text{ Mbar}$. In both studies, chemical analysis was done at room- PT conditions, San Carlos olivine was used as starting material, and $(\text{Mg},\text{Fe})\text{O}$ was always present. Only in the study by Kobayashi *et al.* [2005] was there complementary in-situ x-ray diffraction confirmation of the synthesized PPv phase assemblage. Neither study performed in-situ analysis of iron's valence state.

[9] In the absence of $(\text{Mg},\text{Fe})\text{O}$, several studies suggest that Fe favors PPv compared to Pv [e.g., Caracas and Cohen, 2005; Tateno *et al.*, 2007; Auzende *et al.*, 2008]. Based on previous Mössbauer measurements on Al-free silicate Pv, approximately 10% of the iron is typically Fe^{3+} [McCammon, 1998]. Therefore, when PPv is formed, 10% Fe^{3+} is already present from the Pv phase. The remaining $\sim 90\%$ Fe^{2+} in Pv would transform into $\sim 30\%$ iron metal and 60% Fe^{3+} at the structural transition to PPv according to equations (1a) and (1b) [Frost *et al.*, 2004; Zhang and Oganov, 2006], thus resulting in the $29 \pm 2\%$ metallic iron phase and 71% Fe^{3+} observed in the SMS time spectra for the PPv phase. Note that if one considers an upper bound of 20% Pv (Figure 2) and equal partitioning of Fe between Pv and PPv, then the iron bound in Pv could contribute at most $\sim 7\%$ metallic iron and $\sim 13\%$ Fe^{3+} (according to equation (1b)) to the SMS signal. Therefore, at least $\sim 22\%$ of the metallic iron phase observed is unequivocally associated with PPv.

[10] If the reaction proceeds according to equations (1a) and (1b) above, the amount of the metallic iron and $\alpha\text{-PbO}_2$ structured SiO_2 phase [Dubrovinsky *et al.*, 1997] in the diffracting volume would be 0.8% and 2.4%, respectively. The metallic iron phase and SiO_2 formed in this reaction (equations (1a) and (1b)) could be poorly crystalline, nano-crystalline, and/or below the current detection limit of high-pressure powder diffraction. However, scanning electron microscopy (SEM) allows one to image features on the 100's of nanometer scale. A LEO 1550VP Field Emission SEM was therefore used to analyze the quenched assemblage from $P = 1.19 \text{ Mbar}$. Analysis by SEM combined with semi-quantitative energy dispersive spectroscopy (EDS) shows a small ($\sim 500 \text{ nm}$) iron-rich cluster within the $(\text{Mg},\text{Fe})\text{SiO}_3$ quenched matrix (Figure 3). A line EDS analysis showed that the Fe content in the cluster-area is 50%, with a precision error of 0.3%. The Fe content in the surrounding area varies from 6% to 10.7%, with similar precision and indications iron migration towards the edge. Distinct areas of SiO_2 enrichment could not be decoupled from the iron-rich and silicate areas, as the excitation volume is $\sim 5 \mu\text{m}^3$ below the surface.

[11] The PPv phase assemblage containing a metallic iron-rich phase presented here represents a likely reaction

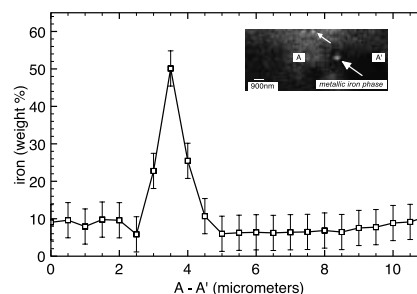


Figure 3. EDS results of the iron content across a trace (A – A' on SEM image inset) in the recovered quenched PPv phase assemblage. The inset SEM image shows the amorphous quenched PPv and an iron-rich cluster (bright spots). Accounting for geometry and excitation volume uncertainties, the errors in composition are likely to be on the order of 10%.

pathway to the higher *PT* assemblages suspected at the core-mantle boundary region. The co-existence of other likely components, namely (Mg,Fe)O, CaSiO₃ perovskite, alumina, and partial melts should have an effect on this reaction process. The presence and composition of metallic iron-rich clusters in the reaction pathway from Pv to PPv should provide insights into the compositional evolution of this region.

[12] **Acknowledgments.** We thank J. Zhao for technical assistance, D. Stevenson for discussions, D. Adams and two anonymous reviewers for their comments. Support for this work was provided in part by the National Science Foundation (NSF) EAR 0711542 and Caltech (J.M.J.), NSF-EAR 0552010 and NNSA Cooperative Agreement DOE-FC52-06NA27684 (O.T.), the U.S. DOE, Office of Science, BES under DE-AC02-06CH11357, and COMPRES under NSF Cooperative Agreement EAR 06-49658. X-ray diffraction experiments were performed at HPCAT (Sector 16, APS). SEM and EDS analyses were carried out at the Caltech GPS Division Analytical Facility (MRSEC Program of the NSF under DMR-0080065).

References

- Alp, E. E., et al. (1995), Synchrotron Mössbauer spectroscopy of powder samples, *Nucl. Instrum. Methods Phys. Res., Sect. B*, *97*, 526–529.
- Auzende, A.-L., et al. (2008), Element partitioning between magnesium silicate perovskite and ferropericlaite: New insights into bulk lower-mantle geochemistry, *Earth Planet. Sci. Lett.*, *269*, 164–174.
- Badro, J., et al. (2003), Iron partitioning in Earth's lower mantle: Toward a deep lower mantle discontinuity, *Science*, *300*, 789–791.
- Badro, J., et al. (2004), Electronic transitions in perovskite: Possible non-convecting layers in the lower mantle, *Science*, *305*, 383–386.
- Caracas, R., and R. E. Cohen (2005), Effect of chemistry on the stability and elasticity of the perovskite and post-perovskite phases in the MgSiO₃-FeSiO₃-Al₂O₃ system and implications for the lowermost mantle, *Geophys. Res. Lett.*, *32*, L16310, doi:10.1029/2005GL023164.
- Crowhurst, J. C., et al. (2008), Elasticity of (Mg,Fe)O through the spin transition of iron in the lower mantle, *Science*, *319*, 451–453.
- DeWaele, A., et al. (2004), Equations of state of six metals above 94 GPa, *Phys. Rev. B*, *70*, 094112, doi:10.1103/PhysRevB.70.094112.
- Dubrovinsky, L., et al. (1997), Experimental and theoretical evidence of a new high-pressure phase of silica, *Nature*, *388*, 362–365.
- Dyar, M. D., et al. (2006), Mössbauer spectroscopy of Earth and planetary materials, *Annu. Rev. Earth Planet. Sci.*, *34*, 83–125.
- Fei, Y., et al. (2007), Toward an internally consistent pressure scale, *Proc. Natl. Acad. Sci. U. S. A.*, *104*, 9182–9186.
- Frost, D. J., et al. (2004), Experimental evidence for the existence of iron-rich metal in the Earth's lower mantle, *Nature*, *428*, 409–412.
- Gaffney, E. S., and D. L. Anderson (1973), Effect of low-spin Fe²⁺ on the composition of the lower mantle, *J. Geophys. Res.*, *78*, 7005–7014.
- Hawthorne, F. C. (1988), Mössbauer spectroscopy, *Rev. Mineral.*, *18*, 255–340.
- Hernlund, J. W., et al. (2005), A doubling of the post-perovskite phase boundary and structure of the Earth's lowermost mantle, *Nature*, *434*, 882–886.
- Jackson, J. M., et al. (2005), A synchrotron Mössbauer spectroscopy study of (Mg,Fe)SiO₃ perovskite up to 120 GPa, *Am. Mineral.*, *90*, 199–205.
- Jackson, J. M., et al. (2009), Nuclear resonant X-ray spectroscopy of (Mg,Fe)SiO₃ orthoenstatites, *Eur. J. Mineral.*, in press.
- Kobayashi, Y., T. Kondo, E. Ohtani, N. Hirao, N. Miyajima, T. Yagi, T. Nagase, and T. Kikegawa (2005), Fe-Mg partitioning between (Mg,Fe)SiO₃ post-perovskite, perovskite, and magnesiowüstite in the Earth's lower mantle, *Geophys. Res. Lett.*, *32*, L19301, doi:10.1029/2005GL023257.
- Lassak, T. M., et al. (2007), Influence of thermochemical piles on topography at Earth's core–mantle boundary, *Earth Planet. Sci. Lett.*, *261*, 443–455.
- Lauterbach, S., et al. (2000), Mössbauer and ELNES spectroscopy of (Mg,Fe)(Si,Al)O₃ perovskite: A highly oxidized component of the lower mantle, *Contrib. Mineral. Petrol.*, *138*, 17–26.
- Li, J., et al. (2006), Pressure effect on the electronic structure of iron in (Mg,Fe)(Si,Al)O₃ perovskite: A combined synchrotron Mössbauer and X-ray emission spectroscopy study up to 100 GPa, *Phys. Chem. Miner.*, *33*, 575–585, doi:10.1007/s00269-00006-00105-y.
- Lin, J.-F., et al. (2005), Spin transition of iron in magnesiowüstite in the Earth's lower mantle, *Nature*, *436*, 377–380.
- Lin, J.-F., et al. (2006a), Pressure-induced electronic spin transition of iron in magnesiowüstite (Mg,Fe)O, *Phys. Rev. B.*, *73*, 113107, doi:10.1103/PhysRevB.73.113107.
- Lin, J.-F., et al. (2006b), Sound velocities of ferropericlaite in the Earth's lower mantle, *Geophys. Res. Lett.*, *33*, L22304, doi:10.1029/2006GL028099.
- Lin, J.-F., et al. (2008), Intermediate-spin ferrous iron in lowermost mantle post-perovskite and perovskite, *Nat. Geosci.*, *1*, 688–691.
- Mao, W. L., et al. (2004), Ferromagnesian postperovskite silicates in the D'' layer of the Earth, *Proc. Natl. Acad. Sci. U. S. A.*, *101*, 15,867–15,869.
- McCammon, C. A. (1997), Perovskite as a possible sink for ferric iron in the lower mantle, *Nature*, *387*, 694–696.
- McCammon, C. A. (1998), The crystal chemistry of ferric iron in Fe_{0.05}Mg_{0.95}SiO₃ perovskite as determined by Mössbauer spectroscopy in the temperature range 80–293 K, *Phys. Chem. Miner.*, *25*, 292–300.
- McCammon, C. (2006), Microscopic properties to macroscopic behavior: The influence of iron electronic state, *J. Mineral. Petrol.*, *101*, 130–144.
- McCammon, C., et al. (2008), Stable intermediate-spin ferrous iron in lower-mantle perovskite, *Nat. Geosci.*, *1*, 684–687.
- Murakami, M., et al. (2004), Post-perovskite phase transition in MgSiO₃, *Science*, *304*, 855–858.
- Murakami, M., et al. (2005), Post-perovskite phase transition and mineral chemistry in the pyrolytic lowermost mantle, *Geophys. Res. Lett.*, *32*, L03304, doi:10.1029/2004GL021956.
- Nakagawa, T., and P. J. Tackley (2004), Effects of a perovskite-post perovskite phase change near core-mantle boundary in compressible mantle convection, *Geophys. Res. Lett.*, *31*, L16611, doi:10.1029/2004GL020648.
- Oganov, A. R., and S. Ono (2004), Theoretical and experimental evidence for a post-perovskite phase of MgSiO₃ in Earth's D'' layer, *Nature*, *430*, 445–448.
- Oganov, A. R., et al. (2005), Anisotropy of Earth's D'' layer and stacking faults in the MgSiO₃ post-perovskite phase, *Nature*, *438*, 1142–1144.
- Pipkorn, D. N., et al. (1964), Mössbauer effect in iron under very high pressure, *Phys. Rev. A*, *135*, 1604–1612.
- Shannon, R. D., and C. T. Prewitt (1969), Effective ionic radii in oxides and fluorides, *Acta Crystallogr., Sect. B Struct. Crystallogr. Cryst. Chem.*, *25*, 925–946.
- Shim, S.-H., et al. (2004), Stability and crystal structure of MgSiO₃ perovskite to the core-mantle boundary, *Geophys. Res. Lett.*, *31*, L10603, doi:10.1029/2004GL019639.
- Sidorin, I., et al. (1999), Evidence for a ubiquitous seismic discontinuity at the base of the mantle, *Science*, *286*, 1326–1331.
- Sinmyo, R., et al. (2006), Ferric iron in Al-bearing post-perovskite, *Geophys. Res. Lett.*, *33*, L12S13, doi:10.1029/2006GL025858.
- Sinmyo, R., et al. (2008a), Partitioning of iron between perovskite/postperovskite and ferropericlaite in the lower mantle, *J. Geophys. Res.*, *113*, B11204, doi:10.1029/2008JB005730.
- Sinmyo, R., et al. (2008b), Ferric iron content in (Mg,Fe)SiO₃ perovskite and post-perovskite at deep lower mantle conditions, *Am. Mineral.*, *93*, 1899–1902.
- Sturhahn, W. (2000), CONUSS and PHOENIX: Evaluation of nuclear resonant scattering data, *Hyperfine Interact.*, *125*, 149–172.
- Tateno, S., et al. (2007), Solubility of FeO in (Mg,Fe)SiO₃ perovskite and the post-perovskite phase transition, *Phys. Earth Planet. Inter.*, *160*, 319–325.
- Tschauner, O., et al. (2008), Possible structural polymorphism in Al-bearing magnesiumsilicate post-perovskite, *Am. Mineral.*, *93*, 533–539.
- van der Hilst, R. D., et al. (2007), Seismostratigraphy and thermal structure of Earth's core-mantle boundary region, *Science*, *315*, 1813–1817.
- Zhang, F., and A. R. Oganov (2006), Valence state and spin transitions of iron in Earth's mantle silicates, *Earth Planet. Sci. Lett.*, *249*, 436–443.

Y. Fei, Geophysical Laboratory, Carnegie Institution of Washington, 5251 Broad Branch Road, NW, Washington, DC 20015, USA.

J. M. Jackson, Seismological Laboratory, Division of Geological and Planetary Sciences, California Institute of Technology, M/C 252-21, 1200 E. California Boulevard, Pasadena, CA 91125, USA. (jackson@gps.caltech.edu)

M. Lerche, HPSynC, Argonne National Laboratory, 9700 South Cass Avenue, Argonne, IL 60439, USA.

W. Sturhahn, Advanced Photon Source, Argonne National Laboratory, 9700 South Cass Avenue, Argonne, IL 60439, USA.

O. Tschauner, High Pressure Science and Engineering Center, Department of Physics, University of Nevada, Box 454002, 4505 Maryland Parkway, Las Vegas, NV 89154, USA.